First-principles calculations of the electronic properties of 3d transition-metal impurities in Al

1991 J. Phys.: Condens. Matter 3 3285

(http://iopscience.iop.org/0953-8984/3/19/007)

J. Phys.: Condens. Matter 3 (1991) 3285–3300. Printed in the UK

First-principles calculations of the electronic properties of 3d transition-metal impurities in Al

Prabhakar P Singh†
Department of Physics and Astronomy, University of North Carolina, Chapel Hill, NC 27514, USA

Received 16 August 1990, in final form 11 January 1991

Abstract. A comprehensive study of 3d transition-metal impurities in Al is carried out using the self-consistent Green function linear-muffin-tin-orbital method. Using the self-consistent potential at the impurity site we investigate the changes in the local density of states and the charge transfer between the impurity and the neighbouring host atoms. The movement of the virtual bound states and the phase shifts at the Fermi energy are used to explain the transport properties of these alloys. For several alloys our results for the impurity resistivities, the thermoelectric powers, the Dingle temperatures and the electronic specific heats are in good agreement with experimental data and the results of other calculations.

1. Introduction

A better understanding of the effects of impurities in solids is essential for an accurate characterization of the electronic properties of real materials. The bulk electronic properties of solids are greatly affected and, at times, entirely determined by the impurities. The presence of an impurity in an otherwise perfect solid destroys the translational symmetry so that the usual k-space methods are not directly applicable for determining the electronic structure of these dilute alloys. The simplest as well as the most successful approach uses the perturbation theory for solving the dilute alloy problem.

Friedel [1, 2] was the first to use the virtual bound-state model to explain the transport properties of dilute alloys. Other approaches for describing the dilute alloys include the Anderson impurity model [3], the localized interaction model of Wolff [4] and the localized spin-fluctuation model [5]. The method for describing the electronic structure of alloys using the Green function approach, suggested by Beeby [6], was simplified and applied to study Ni in Cu alloys by Harris [7]. In the last 10 years Podloucky *et al* [8], Deutz *et al* [9] and Braspenning *et al* [10] have used this approach to study 3d transition-metal as well as s–p impurities in Al and Cu. Results of [9] and [10] are in good agreement with the experimental data, indicating the accuracy of the Green function Korringa–Kohn–Rostoker (KKR) approach.

† Present and permanent address: Department of Materials Science and Mineral Engineering, University of California, Berkeley, CA 94720, USA.

0953-8984/91/193285 + 16 $03.50

As an accurate and realistic description of the alloy requires an accurate description of the electronic structure of the solid that acts as the host to the impurity, any improvement in the description of the solid should result in a better understanding of the alloys. The development of the linear-muffin-tin-orbital (LMTO) method as an accurate and efficient tool for describing the electronic structure of solids led Koenig and coworkers [11–14] and Gunnarsson *et al* [15] to reformulate the Green function KKR method in terms of the LMTO method. We call this approach the Green function LMTO method. Because of the energy linearization and the inclusion of the atomic sphere approximation, the Green function LMTO method is much more efficient than the Green function KKR method, and is almost as accurate.

Koenig and coworkers have carried out self-consistent calculations for Mg, Cu and Zn in Al as well as impurities in Fe and in ordered metallic compounds [11–14]. In their calculations for impurities in Al, only the impurity cell potential is perturbed and the Friedel sum rule is always enforced by adding a constant potential. Their results give a good description of the charge redistribution around the impurity cell. Since its development, the Green function LMTO approach formulated by Gunnarsson *et al* have been successfully applied to impurities in semiconductors [16].

In our opinion, a comprehensive and systematic study of changes in many transport properties, such as the impurity resistivity, the thermoelectric power, the Dingle temperature and the electronic specific heat of the alloys, especially Al-based, is still lacking. Although Koenig *et al* recognized the need for employing more than one energy panel for calculating the Green function at the impurity site, a systematic comparison of results with different number of energy panels is clearly needed. Also, the effects of enforcing the Friedel sum rule on the calculated electronic properties, with only one perturbed muffin tin, may not be justified. The neglect of lattice relaxation around the impurity atom, especially when impurity and host atoms are very different in sizes, may become questionable. Since most of these approximations depend on the electronic structure of the impurity atom, a study based on different impurity atoms is important for a clear understanding of the effects of these approximations on the calculated transport properties.

In an attempt to remedy some of the problems outlined above, we have carried out a detailed study of the electronic properties of 3d transition-metal impurities in Al using the Green function LMTO method. The effects on the calculated transport properties of enforcing the Friedel sum rule and that of more than one energy panel are fully investigated. Since we perturb only the impurity cell potential and ignore the lattice relaxation around the impurity atom, we point out the alloys and the electronic properties for which these might be important. We consider only dilute alloys, meaning that the impurities in the solid do not interact with each other. This is ensured by considering a single impurity atom in an otherwise perfect solid.

The paper is organized as follows. The method used for calculating the electronic structure of the host solid is indicated in section 2.1. Friedel sum rule and its implications are described in section 2.2. Approximations of the Green function LMTO approach are described in section 2.3. Section 3 contains a detailed account of our results in terms of the local density of state, charge transfer, virtual and bound states, impurity resistivity, thermoelectric power, Dingle temperature and electronic specific heat for 3d transition-metal impurities in Al. Finally, after summarizing our work, we describe our conclusions in section 4.

2. Green function LMTO method

For solving the alloy problem we first have to obtain the electronic structure of the host solid and then replace one of the host atoms by an impurity and express the perturbed

lattice Green function in terms of the unperturbed lattice (host solid) Green function and the perturbing potential. The resulting perturbation series can be summed exactly for a localized perturbation. The assumption that only the impurity site potential is perturbed greatly simplifies the summation of the perturbation series. In the following we give a very brief description of the Green function LMTO method. The details can be found in [11–13] and [17].

2.1. Green function at the impurity site

The electronic structure of the host solid is calculated with the LMTO method described in detail by Andersen and coworkers [18, 19]. Then under the assumptions that the perturbing potential is localized within the central cell, the lattice has cubic symmetry, and the angular momentum $l \leqslant 2$, the perturbed lattice Green function at the impurity site, $G(\boldsymbol{r}, \boldsymbol{r}, E)$, is

$$G(\boldsymbol{r}, \boldsymbol{r}, E) = \sum_L \frac{\varphi_l^2(r, E_l^*) Y_L^2(\hat{r})}{E - E_l^*} + \sum_L \dot{P}_l(E) \varphi_l^2(r, E) Y_L^2(\hat{r}) \left(\frac{1}{P_l(E) - \bar{P}_l(E) + \Sigma_{LL}^{-1}} - \frac{1}{P_l(E)} \right) \tag{1}$$

where $\varphi_l(r, E)$ are the partial-wave solutions for the impurity potential, normalized to unity within the Wigner–Seitz (ws) sphere. The potential functions of the host and the impurity are denoted by $\bar{P}_l(E)$ and $P_l(E)$ respectively, $Y_L(\hat{r})$ are the cubic harmonics, $L \equiv (l, m)$ is the orbital index, and E_l^* represents the lth bound state of the impurity potential. Σ_{LL} is defined in [13] and [17]. Throughout, we denote quantities related to the host solid by an overbar and an energy derivative by an overdot. Once the perturbed lattice Green function at the impurity site is known, all relevant quantities can be easily evaluated.

The electronic density of states, $n_L(E)$, can be written as

$$n_L(E) = -\frac{\dot{P}_l(E)}{\pi} \frac{\operatorname{Im} \Sigma_{LL}(E)}{[1 + \operatorname{Re} \Sigma_{LL}(E) \Delta P_l(E)]^2 + [\operatorname{Im} \Sigma_{LL} \Delta P_l(E)]^2} \tag{2}$$

with

$$\Delta P_l(E) = P_l(E) - \bar{P}_l(E) \tag{3}$$

being the difference between the potential functions of the impurity and the host atoms. For the potential functions we use the *third*-order approximation as given in [18]. The partial waves $\varphi_l(r, E)$ are approximated by their Taylor series expansion around E_{vl} with terms up to *second* order in $(E - E_{vl})$.

We see from equation (2) that the impurity density of states is maximum whenever

$$1 + \operatorname{Re} \Sigma_{LL}(E) \Delta P_l(E) = 0 \tag{4}$$

for some $E = E_l^{\dagger}$. The energy $E_l^{\dagger}$ at which the resonance can occur is determined by the parameter $\Delta P_l(E)$ defined in equation (3). Depending upon the value of the parameter

$\Delta P_l(E)$, the impurity density of states $n_L(E)$ will show virtual or localized levels or no distinguishable change.

2.2. *Friedel sum rule*

A criterion for self-consistent calculations can be easily derived by considering the changes in the integrated density of states and the Friedel sum rule [8]. According to the Friedel sum rule, the changes in the integrated density of states should equal the number of electrons to be accommodated within the Fermi energy of the host crystal. The total change in the integrated density of states, $\Delta N(E)$, is

$$\Delta N(E) = \frac{1}{\pi}\sum_L [\delta_l(0) - \bar{\delta}_l(0)] + \frac{1}{\pi}\sum_L \Delta_L(E) \tag{5}$$

where $\delta_l(0)$ and $\bar{\delta}_l(0)$ are the phase shifts due to isolated muffin-tin potentials of the impurity and of the host atoms embedded in free space respectively, and

$$\tan \Delta_L(E) = \frac{-\operatorname{Im} \Sigma_{LL}(E)\Delta P_l(E)}{1 + \operatorname{Re} \Sigma_{LL}(E)\Delta P_l(E)}. \tag{6}$$

We can define a total phase shift, $\eta_L(E)$, also called the generalized Friedel phase shift, such that

$$\Delta N(E) = \frac{1}{\pi}\sum_L \eta_L(E). \tag{7}$$

Equation (7) describes, in terms of the total phase shift $\eta_L(E)$, the total charge displaced up to energy E when an impurity atom is introduced in an otherwise perfect crystal. According to the Friedel sum rule, the total displaced charge up to the Fermi energy should equal the difference in the atomic numbers of the impurity and the host atoms, i.e.

$$\Delta N(E_F) = Z - \bar{Z} \tag{8}$$

where Z and $\bar{Z}$ are the atomic numbers of the impurity and the host atoms respectively. Thus for complete screening, with one perturbed WS cell, we must have

$$N_{loc} = \Delta N(E_F) + \bar{Z} \tag{9}$$

where N_{loc} is the charge inside the impurity WS sphere. Defining

$$N_{tot} \equiv \Delta N(E_F) + \bar{Z} \tag{10}$$

we see that the screening rule, given by equation (8), becomes

$$N_{tot} = Z. \tag{11}$$

When we do not enforce the Friedel sum rule by adding a constant potential, $V_M(r)$, then a comparison between N_{tot}, calculated by equation (10), and Z indicates the kind of screening achieved.

2.3. *Approximations*

There are essentially four most important approximations in the Green function LMTO method. They are: (i) asssumption of a localized perturbation, (ii) approximate parametrization of the potential function, (iii) lack of combined correction terms [13, 18],

Table 1. Comparison of results for Al obtained by LMTO method with combined correction terms and Green function LMTO method with four energy panels and without the combined correction terms. Density of states is in states Ryd^{-1} $atom^{-1}$.

	LMTO	g2
V_{MTZ} (Ryd)	−0.716	−0.714
Number of s electrons	1.130	1.126
Number of p electrons	1.451	1.462
Number of d electrons	0.419	0.417
s density of states at E_F	1.140	1.163
p density of states at E_f	2.559	2.606
d density of states at E_F	1.610	1.600

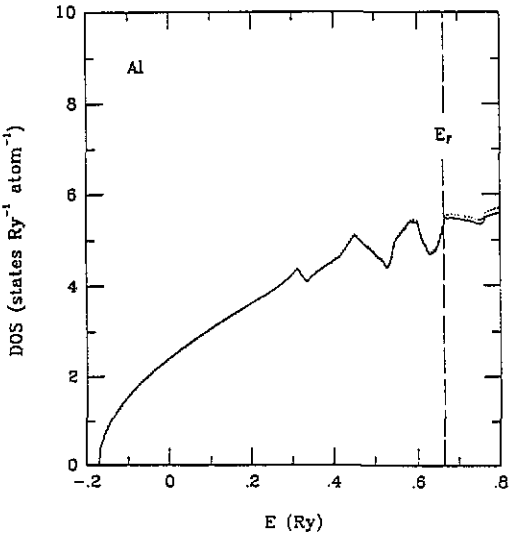

Figure 1. Comparison of local density of states for Al in Al calculated with the Green function LMTO method (four energy panels and $V_M(r) = 0$; dotted curve) with the density of states obtained from the LMTO method (full curve).

and (iv) finite basis approximation. The implications as well as ways to improve upon these approximations are indicated below.

We assume that the impurity potential is localized within a single ws cell. This approximation simplifies the calculation considerably, but to be able to predict charge transfer between the impurity and the nearest-neighbour host atoms more accurately we should extend the perturbation to at least the nearest-neighbour cells. The introduction of nearest-neighbour perturbation is not expected to change the trend in the charge transfers obtained with one perturbed ws cell.

An accurate expression for the potential function is necessary to describe the impurity electronic structure reliably. We parametrize the potential functions as described in [13], [17] and [18]. Around $E = E_l^*$ we use a linear approximation for the potential

functions. For determining E_l^*, also denoted by C_l, we use the second-order approximation

$$E_l^* = E_{vl} + \omega_l(-) \tag{12}$$

where $\omega_l(-)$ is defined in [18].

The electronic structure of the host is calculated with the LMTO method, including the combined correction terms [18]. We do not use the combined correction terms in the impurity potential. To show that the lack of combined correction terms in the impurity atom Hamiltonian does not introduce a significant error in the calculation we used an Al atom as an impurity in Al host. The calculation was carried out with four energy panels. The results of our calculation for Al in Al using the Green function LMTO method are compared with the results for bulk Al obtained from the LMTO method in table 1. The remarkable agreement between the results obtained with the two methods confirms the accuracy of the Green function LMTO approach. In figure 1, the local densities of states are compared with the densities of states obtained with the LMTO method. The Green function LMTO density of states essentially reproduces the density of states obtained for bulk Al using the LMTO method with combined correction terms.

The use of a limited number of angular momenta introduces a small error in the description of the electronic structure of the impurity. We use angular momenta up to $l = 2$, which results in diagonal matrix elements for the Green function of the host. Since the impurity atoms have strong d-character, the neglect of higher angular momentum components is not expected to affect the results considerably.

3. Results and discussion

The self-consistent electronic structure of 3d transition-metal impurities in Al is calculated under three different conditions to serve as test cases for different levels of approximations made in the Green function LMTO method. The calculations are carried out using: (i) one energy panel with $V_M(r) = 0$, (ii) four energy panels with $V_M(r) = 0$, and (iii) four energy panels with $V_M(r) \neq 0$. In (i) and (ii) the Friedel sum rule is not enforced. In (iii) a constant potential is added such that the screening rule is satisfied. For convenience, we denote calculations done with (i), (ii) and (iii) by g1, g2 and g3 respectively.

The atomic wavefunctions of the impurity and host atoms are calculated by solving, self-consistently, the fully relativistic Dirac equation with free-atom boundary conditions. The electronic configurations of atoms belonging to the 3d series of the periodic table are listed in table 1 of [17]. During the self-consistent Green function LMTO calculations we freeze the potential due to all core electrons. The exchange and correlation effects are included through the parametrization given by von Barth and Hedin [20].

To account for some of the approximations mentioned in section 2.3, we include the combined correction terms [18, 19] for calculating the electronic structure of bulk Al. The Brillouin zone integration was carried out with 916 points in the irreducible wedge of the Brillouin zone and the reference energy E_{vl} was chosen to be the centre of gravity of the occupied part of the l band.

Below we present a detailed account of our results for the electronic properties of 3d transition-metal impurities in Al calculated with the Green function LMTO method. The results have been collected under the following categories: (i) local density of states,

(ii) charge transfer and screening, (iii) virtual and bound states, (iv) impurity resistivity, (v) thermoelectric power, (vi) Dingle temperature and (vii) electronic specific heat.

It is obvious that the Green function LMTO method with four energy panels is more accurate than with one energy panel. Results obtained by enforcing the Friedel sum rule should also give better results, since we know that the impurity is completely screened in the metal. The constant potential that has to be added for satisfying the sum rule converges quickly to a stable value for most impurities. The problem arises when there is a large density of states at E_F so that a small change in the constant potential results in a relatively large charge transfer. We find this to be true in the case of AlCr and AlMn. The perturbation of only the impurity muffin tin and the subsequent enforcing of the Friedel sum rule may not be appropriate in those cases where the perturbation on the neighbouring atoms is appreciable. Thus, in the following, we quote results obtained with different approximations (g1, g2 and g3) but concentrate on the results obtained with the four energy panels and $V_M(r) = 0$, i.e. g2.

3.1. Local density of states

For dilute metallic alloys, where the impurity is quickly screened, the most dominant change in the local density of states occurs at the impurity site; hence as a first approximation it is reasonable to assume that host atoms surrounding the impurity remain bulk-like. The perturbation of nearest-neighbour atoms, which results in a substantial increase in the computational effort, is not required because the central site perturbation predicts results that are in good agreement with the experiments.

In figure 2 we show the local densities of states (DOS) for 3d transition-metal impurities in Al calculated with g1. These local densities of states can be easily understood in terms of the bulk density of states and the idea of resonance and anti-resonance points. By comparing the s and p densities of states of the impurity with the corresponding densities of states of bulk Al, we find that the impurity densities of state have all the structures of the bulk DOS but are at least a factor of 3–4 smaller [17]. The s and p densities of states do not change much as we go through AlTi to AlCu. The d density of states at the impurity site is also similar to the bulk Al d density of states, except around the virtual bound states that extend from $E = 0.3$ Ryd onwards for AlTi. The movement of the virtual bound state from well outside the Fermi energy for AlTi to well inside for AlCu can be seen clearly. We also see that the virtual bound states deviate appreciably from the Lorentzian shape [9].

The use of more than one energy panel improves the accuracy of the results because of our linear approach, although the difference in the local density of states calculated with one energy panel and four energy panels is appreciable only around the resonant level as shown in figure 3. Except for AlCu, the largest difference in the local density of states due to g1 and g2 occurs for AlNi, which is less than 2 states/Ryd around the virtual bound state where the density of states is more than 100 states/Ryd. In the case of AlCu, the difference in the position of the virtual bound state is relatively large (0.3 mRyd) and since the density of states is very high, the difference in DOS due to g1 and g2 is also relatively large. Thus, when the resonant level is close to the Fermi energy, as for AlCr, AlMn and AlFe, one must use more than one energy panel with one energy panel close to the Fermi energy. This enables an accurate evaluation of relevant quantities at the Fermi energy which are used for describing the transport properties of alloys.

For satisfying the Friedel sum rule, we add a constant potential $V_M(r)$, which essentially shifts the density of states calculated without $V_M(r)$. The resulting differences in

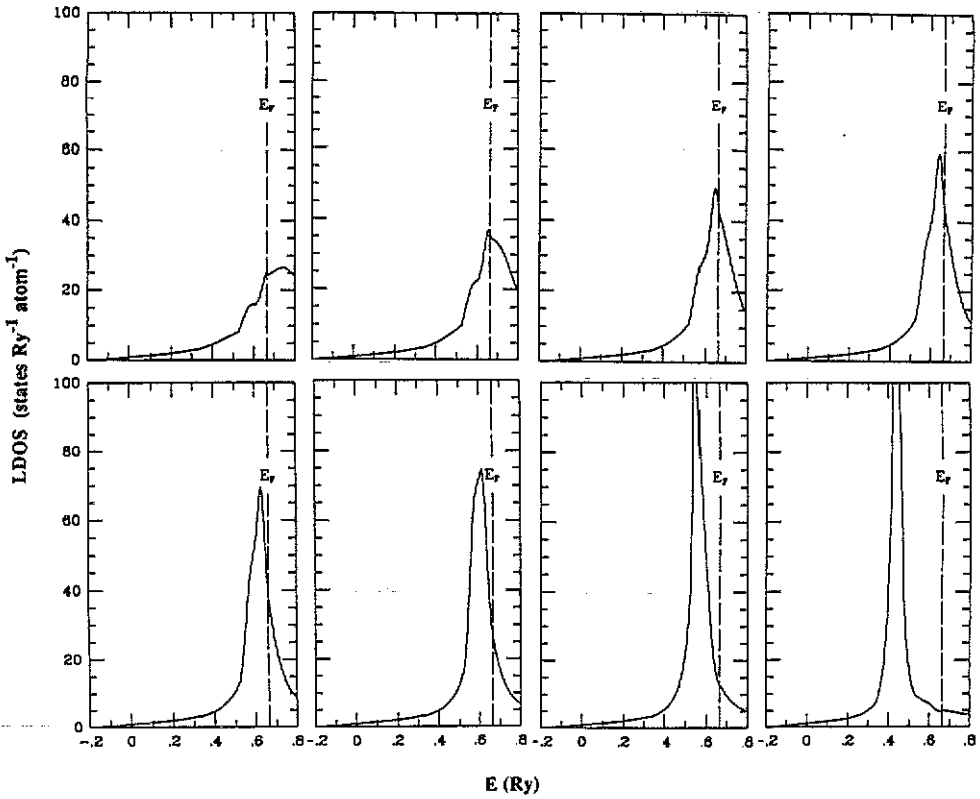

Figure 2. Total local densities of states for 3d transition-metal impurities in Al using the Green function LMTO method with one energy panel and Madelung constant $V_M(r) = 0$ (g1). Top row: Ti, V, Cr and Mn; bottom row: Fe, Co, Ni and Cu.

DOS for AlTi, AlCr and AlCu are shown in figure 3. Since we perturb only the impurity site and do not take into account the lattice relaxation effects, enforcing of the Friedel sum rule should be done with care. This is especially true if the impurity and host atoms are of very different sizes, for example Co and Ni in Al.

3.2. Charge transfer and screening

The amount of charge in the impurity ws sphere and the total charge for 3d impurities in Al are given in table 2. The results for N_{loc} obtained from g1 and g2 are very similar, but the results obtained by enforcing the Friedel sum rule are slightly different. All 3d impurities, except Ti, gain some charge from their neighbouring Al atoms. A similar trend in charge transfer was also found by Deutz *et al* [9]. The total valence charge, given by N_{tot}, is always larger than Z (except for Cr and Mn) for all the impurities. The discrepancy in the values for Cr and Mn is due to the presence of the virtual bound state near E_F. For complete screening, with only one perturbed muffin tin, N_{tot} should equal Z, i.e. the impurity is fully screened within the ws sphere. Deviations from this equality for calculations with g1 and g2 indicate the need for enforcing the Friedel sum rule as well as perturbing at least the nearest neighbours of the impurity atom. Calculations done with g3 clearly demonstrate the need for perturbing the nearest neighbours of the

Table 2. Results for N_{loc} and N_{tot} for impurities in Al using Green function LMTO method with different approximations (g1, g2 and g3). Full screening within the impurity ws sphere implies $N_{tot} = Z$.

		N_{loc}			N_{tot}		
Impurity	Z	g1	g2	g3	g1	g2	g3
Al	3		3.004			3.002	
Ti	4	3.988	3.987	3.480	4.617	4.626	4.000
V	5	5.090	5.088	4.538	5.631	5.641	5.001
Cr	6	6.185	6.179	6.738	2.583	2.598	3.440
Mn	7	7.242	7.232	7.899	−2.507	−2.492	2.062
Fe	8	8.293	8.279	7.895	8.388	8.402	8.000
Co	9	9.326	9.309	9.045	9.278	9.289	9.017
Ni	10	10.333	10.316	10.192	10.168	10.178	10.049
Cu	11	11.277	11.273	11.103	11.070	11.078	10.888

impurity because, although the sum rule is satisfied, the local valence charge is different than Z.

We also find that for AlCr and AlMn the Fermi energy lies in the middle of the crystal-field-split virtual bound states. The presence of the Fermi energy near the virtual bound states creates some problems when we are trying to enforce the Friedel sum rule. To circumvent the problem, one can consider the weighted average of e_g and t_{2g} projected densities of states or use a complex energy grid. We do not follow these procedures; hence our values for the total charge in the case of AlCr and AlMn are not accurate.

3.3. Virtual and bound states

We use the self-consistent Green function LMTO results and equation (4) to calculate the positions of the virtual bound states (VBS). For calculating the positions of the d virtual level, we take the weighted average of the symmetry-projected densities of states and its Hilbert transforms and then use equation (4) with $L \equiv$ d. The virtual level, E_d, is essentially given by

$$E_d = \tfrac{2}{5}E_{e_g} + \tfrac{3}{5}E_{t_{2g}}. \tag{13}$$

The movement of the virtual levels in Al can be understood by considering the filling up of the atomic d level of the impurity atom. For example, let us consider the movement of the virtual levels for 3d impurities in Al. The atomic d level of Ti with its two d electrons is well above E_F of Al. Thus, the corresponding VBS is also well above E_F but with its position changed due to the interaction with the host atoms. As we add more electrons to the d orbital and increase the nuclear charge, the atomic d level lowers its energy, resulting in movement of the VBS towards E_F. The virtual bound state crosses E_F between AlCr and AlMn and it is well inside for AlCu.

Since the half-widths, Γ, are much larger than the crystal-field splitting, it is more appropriate to discuss the virtual bound states E_d rather than E_{e_g} and $E_{t_{2g}}$. In table 3 the virtual bound states E_d and the half-widths for 3d impurities in Al are given. We have also listed the results of Deutz *et al* [9], as well as experimental values. The virtual d level for Ti is about 131 mRyd above E_F while for Cu it is about 222 mRyd below.

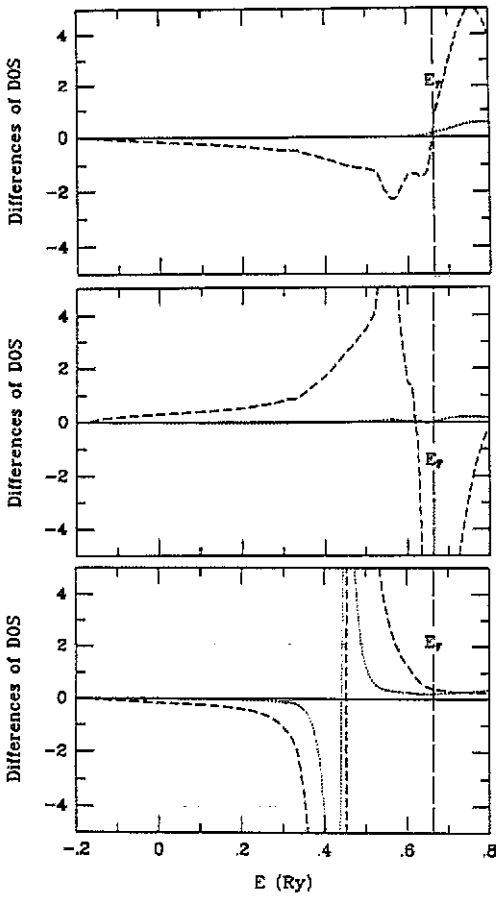

Figure 3. Differences in the total LDOS due to four energy panels with $V_M(r) = 0$ and g1 (dotted curve), and four energy panels with $V_M(r) \neq 0$ and g1 (broken curve) for AlTi (upper frame), AlCr (middle frame) and AlCu (lower frame).

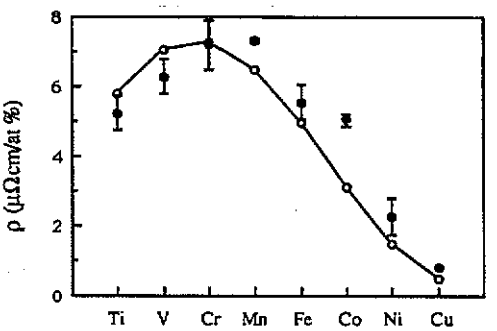

Figure 4. Impurity resistivities for 3d impurities in Al (open circles connected by the full lines) calculated with the Green function LMTO method. Full circles are measurements of Babic *et al* [22].

Table 3. Virtual levels E_d, measured with respect to Fermi energy, and the associated half-widths Γ for impurities in Al using the Green function LMTO method (g2) compared with experimental values (a) and theoretical calculation of [7] (b).

	E_d (mRyd)			2Γ (mRyd)		
Impurity	g2	b	a	g2	b	a
Ti	131.7	73.52			418.9	
V	58.9	0.0		288.4	249.8	
Cr	13.0	−22.00		266.1	213.1	
Mn	−13.4	−44.10	−51.47	108.9	169.0	102.8
Fe	−29.7	−58.80	−66.17	87.2	146.9	110.2
Co	−50.4	−80.88	−110.29	84.6	110.2	117.5
Ni	−101.3	−132.25	−176.47	65.2	44.0	88.1
Cu	−222.2	−227.94	−330.88	47.0	51.4	80.8

According to our calculations, the virtual d level crosses E_F between Cr and Mn. Our values for the virtual levels are closer to E_F than the experimental values. The largest discrepancy is for the VBS of AlCu.

The values for the half-widths associated with the VBS, given in table 3, clearly show that the crystal-field splitting is swamped by the rsonance. For example, in AlCr the crystal-field splitting, $E_{t_{2g}} - E_{e_g} = 36.4$ mRyd, while the half-width for the corresponding E_d is equal to 133 mRyd. The half-widths indicate that the VBS get narrower as we go from Ti to Cu, which is confirmed by the experiment, as shown for AlMn to AlCu in table 3. The narrowing of the virtual levels can be understood in terms of the filling up of the atomic d orbital of the impurity atom. The increased number of electrons increases the interaction around the resonance energy, which results in the higher densities of states and smaller half-widths as we go from Ti to Cu. Given the fact that our calculation for Γ is approximate, the agreement between our results and experimentally determined values of Γ for AlMn to AlCu is reasonable.

3.4. Impurity resistivity

The impurity resistivity is calculated using the Gupta–Benedek [21] approximation. We replace the atomic phase shifts by the generalized Friedel phase shifts so that the impurity resistivity ρ is given by [8]

$$\rho = \frac{2hc}{\bar{Z}e^2 k_F} \sum_{l=0} (l+1) \sin^2[\eta_{l+1}(E_F) - \eta_l(E_F)] \tag{14}$$

where c is the impurity concentration, h is the Planck's constant, e is the electronic charge and k_F is the Fermi wavevector.

In the Gupta–Benedek approximation, the Fermi surface of the host is assumed to be spherical. To take into account the non-spherical nature of the Fermi surface, one can redefine the effective number of conduction electrons, denoted by $\bar{Z}$ in equation (14). We have used the phase shifts, obtained from equation (7), to calculate the impurity resistivity for 3d impurities in Al.

The calculated impurity resistivity due to 3d impurities in Al are plotted in figure 4. The impurity resistivity due to different calculations (g1, g2 and g3) are not very different and cannot be distinguished with the resolution of figure 4, so we show only the results due to g2. The experimental values, measured by Babic *et al* [22], are also shown. Although the number of conduction electrons for metallic Al is 3 per atom, it can be shown that the effective number of electrons is less than 3. The effective number of free electrons is obtained by comparing the free-electron Fermi surface with that of the actual Fermi surface of Al. The comparison yields 2.187 electrons per Al atom, and we have used $\bar{Z} = 2.187$ for calculating the impurity resistivities. We have seen that the virtual bound states for 3d impurities in Al start out well above E_F for AlTi, cross E_F between AlCr and AlMn, and are well inside for AlCu. Owing to the presence of the VBS near E_F in AlCr, the Fermi electrons are resonantly scattered, with scattering decreasing on either side of Cr in the 3d series. Consequently, the impurity resistivity should show a broad peak with maximum around AlCr. The predicted variation in the impurity resistivity of 3d impurities in Al agrees quite well with the calculated impurity resistivity, as shown in figure 4.

Table 4. Thermoelectric power for 3d impurities in Al calculated using the Green function LMTO method (g2) and experimental results (a). Results calculated using localized spin-fluctuation theory are also given (b^{LSF}).

	S_D/T ($10^{-2}\,\mu V\,K^{-2}$)		
Impurity	g2	b^{LSF}	a
Ti	0.122		0.1
V	−0.156		0.1
Cr	−0.337	−1.755	−0.8
Mn	−0.414	−4.441	−5.9
Fe	−0.396	−1.154	−4.1
Co	−0.206		−2.0
Ni	0.124		−2.0
Cu	0.280		

The calculated resistivities are in good agreement with the experimental values, except for AlCo. The values of the calculated impurity resistivity are expected to be lower than the actual values, because we do not allow for the lattice relaxation or perturbation of the neighbouring atoms. The effect of size differences between the impurity and the host atoms is expected to be the largest for Ni and Co. Inclusion of these effects will lead to increased scattering and hence to higher resistivities.

3.5. Thermoelectric power

To illustrate the limitations of the Friedel–Anderson model for dilute alloys, we have calculated the diffusive thermoelectric power, S_D. At low temperatures, the thermoelectric power of a metal is essentially due to the scattering of electrons by the impurities and it is related to the impurity resistivity by [23]

$$S_D = \frac{\pi^2 k^2 T}{3e} \frac{\partial \ln \rho(E)}{\partial E} \tag{15}$$

where k is the Boltzmann constant. Using equation (14), the expression for S_D can be rewritten as

$$S_D = \frac{\pi^2 k^2 T}{3e}\left[-\frac{1}{2E} + \frac{\sum_{l=0} (l+1)\sin^2(\eta_{l+1}-\eta_l)\left(\frac{\partial \eta_{l+1}}{\partial E} - \frac{\partial \eta_l}{\partial E}\right)}{\sum_{l=0}(l+1)\sin^2(\eta_{l+1}-\eta_l)}\right] \tag{16}$$

which is to be evaluated at E_F. We used equation (16) to calculate the thermoelectric power of 3d impurities in Al. The calculated thermopowers for AlCr, AlMn and AlFe are found to be in strong disagreement with the experimental values, clearly demonstrating the inadequacy of the Friedel–Anderson model. To be able to explain the experimentally observed thermopowers we have to use the localized spin-fluctuation theory as mentioned in section 1.

The impurity contribution to the diffusive thermopower of Al-based alloys is shown in table 4. The large discrepancy between the calculated and the observed thermopowers

Table 5. Dingle temperature for 3d impurities in Al calculated using the Green function LMTO method (g1) compared with the results of [25](a).

	Dingle temperature T_D (K/at.%)	
Impurity	g1	a
Ti	256	289
V	330	347
Cr	365	381
Mn	351	370
Fe	299	318
Co	219	229
Ni	133	139
Cu	64	71

for Cr, Mn and Fe is obvious, which can be explained by using the localized spin-fluctuation (LSF) theory developed by Zlatic and others [5]. In the LSF approach, a sharp resonance due to localized spin fluctuation is set up at E_F. A detailed account of the LSF approach is given by Grüner *et al* [5].

Using a relatively narrow resonance at E_F for Cr, Mn and Fe (the respective widths used are inferred from [5] and are equal to 0.024, 0.01 and 0.04 Ryd respectively) the new calculated thermoelectric powers, shown under column b^{LSF} of table 4, are in good agreement with the observed values. For AlFe, we get a slightly smaller value in magnitude than obtained by Zlatic [5], which is probably due to the positioning of the resonance and the use of an approximate expression by him for evaluating the thermopowers. For simplicity, we have assumed that the resonances due to the spin fluctuations are situated at E_F.

3.6. Dingle temperature

The de Haas–van Alphen (dHvA) effect describes the changes in the electronic energy levels of solids due to the magnetic fields. The presence of an impurity in the solid changes the electronic energy levels and hence affects the dHvA effect. It can be shown that the energy levels become broadened in the presence of the impurities [24]. The broadening of energy levels is described in terms of the Dingle temperature (similar to thermal broadening), T_D, defined as [25]

$$T_D = \frac{4cE_F}{3\pi^2 \bar{Z}k} \sum_{l=0} (2l+1) \sin^2[\eta_l(E_F)]. \tag{17}$$

Equation (17) is derived by assuming an average relaxation time over the Fermi surface. As the Dingle temperature is directly related to the scattering of Fermi electrons, the impurity whose virtual bound state is the closest to the host Fermi energy should have the largest Dingle temperature. This is found to be true for AlCr.

The effect of impurities on electron scattering in a magnetic field can be measured in terms of the Dingle temperature T_D. Our calculated values of the Dingle temperature for 3d impurities in Al are listed in table 5. The Dingle temperature increases from Ti to Cr and then decreases, indicating the amount of effective scattering by each impurity. As expected, the resonant scattering of the Fermi electrons for AlCr leads to the

Table 6. Change in the coefficient of electronic specific heat for 3d impurities in Al calculated using the Green function LMTO method (g1) compared with experimental values (a) taken from [27].

Impurity	g1	a
Ti	0.0308	
V	0.0368	0.22 ± 0.06
Cr	0.0352	0.32 ± 0.06
Mn	0.0252	0.44 ± 0.04
Fe	0.0097	
Co	−0.0093	
Ni	−0.0247	
Cu	−0.0270	

maximum T_D. The amount of scattering decreases on both sides of Cr, which is reflected in the decreased T_D. We have also listed the T_D calculated by Mrosan and Lehmann [25]. Although their calculation is not self-consistent, the agreement is remarkable. We have not been able to find any experimental values for T_D for Al-based alloys.

3.7. Electronic specific heat

The electronic contribution to the specific heat of solids is related to the total density of states at E_F. The coefficient of the electronic specific heat, γ_{el}, is given by [26]

$$\gamma_{el} = \tfrac{1}{3}\pi^2 k^2 n(E_F) \tag{18}$$

where we have ignored the electron–phonon interaction. The impurity changes the density of states at E_F and that changes the electronic contribution to the specific heat of the alloy. The total change in the density of states due to the impurity can be calculated by taking the derivative of equation (18) with respect to energy and evaluating it at E_F, i.e.

$$\Delta n = \frac{d}{dE}[\Delta N(E)]_{E=E_F}. \tag{19}$$

The change in the coefficient of electronic specific heat is given by

$$\Delta\gamma_{el} = c\Delta n(E_F) \tag{20}$$

where c is the impurity concentration.

The calculated changes in the coefficient of the electronic specific heats for 3d impurities in Al are given in table 6. For AlCo, AlNi and AlCu, the change in the coefficients of the specific heat is negative. The values for AlCr and AlMn are uncertain due to the presence of the VBS near E_F in these alloys. The observed values of $\Delta\gamma_{el}$, reported by Aoki and Ohtsuka [27] are higher than our predicted values for AlV, AlCr and AlMn.

4. Summary and conclusions

We have studied Al-based dilute alloys using the Green function LMTO method. For our self-consistent calculations we have assumed that the impurity potential is localized

within the impurity WS sphere. The assumption of only one perturbed muffin tin implies that all the host atoms, including the nearest-neighbour atoms, are taken to be bulk-like. Using the resulting self-consistent potential at the impurity site we have calculated the transport properties such as impurity resistivity, thermoelectric power, Dingle temperature and electronic specific heat for 3d transition-metal impurities in Al.

We find that our results are well described by the Friedel virtual bound-state and Anderson impurity models and these are in excellent agreement with the experimental data. Most of the transport properties of dilute alloys can be explained on the basis of the Friedel–Anderson model. An analysis based on phase shifts up to $l = 2$ is sufficient to account for most of the observed properties. In the case of nearly magnetic alloys, e.g. Cr, Mn and Fe in Al, the explanation of the observed thermoelectric power requires the localized spin-fluctuation model.

The Green function LMTO method is found to be as accurate as the Green function KKR method for describing the transport properties of dilute alloys. From our results we also see that: (i) the lack of combined correction terms in the impurity Hamiltonian introduces negligible error, (ii) the use of more than one energy panel improves the accuracy, and (iii) a careful analysis is needed before enforcing the Friedel sum rule with only one permitted muffin tin.

Our results are based on perturbing only the impurity muffin tin, but, to be able to predict charge transfers between the impurity and the host atoms more accurately, we must perturb at least the nearest-neighbour host atoms. In the Green function LMTO method, the perturbation of the nearest-neighbour atoms leads to a significant increase in the computational effort. In some cases, lattice relaxation may become important.

Acknowledgments

The help and guidance of Professor Kian S Dy and Professor William J Thompson are gratefully acknowledged.

References

[1] Friedel J 1956 *Can. J. Phys.* **34** 1190
[2] Friedel J 1958 *Nuovo Cim. Suppl.* 7 287
[3] Anderson P W 1961 *Phys. Rev.* **124** 41
[4] Wolff P A 1961 *Phys. Rev.* **124** 1030
[5] Grüner G and Zawadowski A 1974 *Rep. Prog. Phys.* **37** 1497
Zlatic V and Rivier N 1974 *J. Phys. F: Met. Phys.* **4** 732
[6] Beeby J L 1967 *Proc. R. Soc.* A **302** 113
[7] Harris R 1970 *J. Phys. C: Solid State Phys.* **3** 172
[8] Podloucky R, Zeller R and Dederichs P H 1980 *Phys. Rev.* B **22** 5777
[9] Deutz J, Dederichs P H and Zeller R 1981 *J. Phys. F: Met. Phys.* **11** 1787
[10] Braspenning P J, Zeller R, Lodder A and Dederichs P H 1984 *Phys. Rev.* B **29** 703
[11] Koenig C, Léonard P and Daniel E 1981 *J. Physique* **42** 1015; Koenig C and Daniel E 1981 *J. Physique* **42** L193
[12] Léonard P and Stefanou N 1985 *Phil. Mag.* B **51** 151
[13] Koenig C, Stefanou N and Koch J M 1986 *Phys. Rev.* B **33** 5307
[14] Koch J M, Stefanou N and Koenig C 1986 *Phys. Rev.* B **33** 5319
[15] Gunnarsson O, Jepson O and Andersen O K 1983 *Phys. Rev.* B **27** 7144
[16] Gunnarsson O, Andersen O K, Jepson O and Zaanen J 1989 *Phys. Rev.* B **39** 1708
[17] Singh P P 1989 *PhD Thesis* University of North Carolina at Chapel Hill (unpublished)

[18] Skriver H L 1984 *The LMTO Method* (Berlin: Springer)
[19] Andersen O K 1975 *Phys. Rev.* B **12** 3060; 1984 *The Electronic Structure of Complex Systems* (NATO Advanced Study Institute, Gent, 1982) ed N Temmerman and P Phariseau (New York: Plenum) p 11
Andersen O K and Jepsen O 1984 *Phys. Rev. Lett.* **53** 2571
Andersen O K, Jepson O and Glötzel D 1985 *Highlights of Condensed Matter Theory* ed F Bassani, F Fumi and M P Tosi (New York: North-Holland)
Andersen O K, Jepson O and Sob M 1987 *Electronic Band Structure and its Applications* ed M Youssouff (Berlin: Springer) p 1
[20] von Barth U and Hedin L 1972 *J. Phys. C: Solid State Phys.* **5** 1629
[21] Gupta R P and Benedek R 1979 *Phys. Rev.* B **19** 583
[22] Babic E, Krsnik R and Rizzuto C 1973 *Solid State Commun.* **13** 1027
[23] Barnard R D 1972 *Thermoelectricity in Metals and Alloys* (London: Taylor and Francis)
[24] Shoenberg D 1984 *Magnetic Oscillations in Metals* (Cambridge: Cambridge University Press)
[25] Mrosan E and Lehmann G 1976 *Phys. Status Solidi* b **78** 159
[26] Papaconstantopoulos D A 1986 *Handbook of the Band Structure of Elemental Solids* (New York: Plenum)
[27] Aoki R and Ohtsuka T 1969 *J. Phys. Soc. Japan* **26** 651